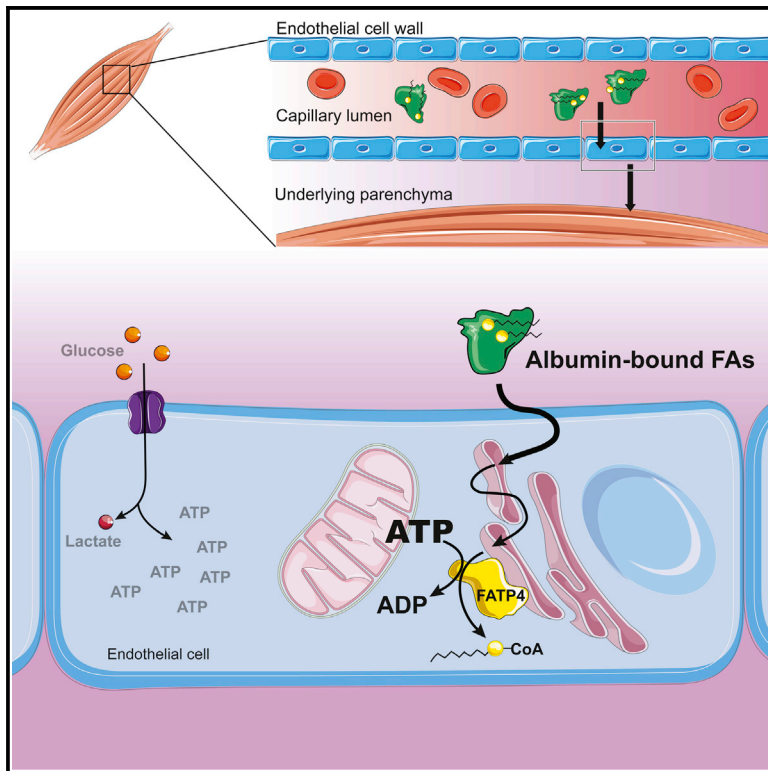


Cell Metabolism

Local Mitochondrial ATP Production Regulates Endothelial Fatty Acid Uptake and Transport

Graphical Abstract



Authors

Ayon Ibrahim, Nora Yucel, Boa Kim, Zoltan Arany

Correspondence

zarany@penmedicine.upenn.edu

In Brief

Ibrahim et al. discover that mitochondrial (but not glycolytic) ATP regulates endothelial fatty acid uptake and transport. Endothelial mitochondria are closely juxtaposed to ER, and ATP locally produced by mitochondria is used by FATP4, which resides in the ER, to promote fatty acid uptake via its ATP-dependent acyl-CoA synthetase activity.

Highlights

- A chemical screen identifies novel inhibitors of endothelial fatty acid uptake
- Endothelial fatty acid uptake and transport requires specifically mitochondrial ATP
- Endothelial mitochondria are proximally positioned to the ER
- ER-borne FATP4 uses mitochondrial ATP to mediate vectorial acylation of fatty acids

Short Article

Local Mitochondrial ATP Production Regulates Endothelial Fatty Acid Uptake and Transport

Ayon Ibrahim,¹ Nora Yucel,¹ Boa Kim,¹ and Zoltan Arany^{1,2,*}

¹Cardiovascular Institute, Perelman School of Medicine, University of Pennsylvania, Philadelphia, PA 19104, USA

²Lead Contact

*Correspondence: zarany@penncmedicine.upenn.edu

<https://doi.org/10.1016/j.cmet.2020.05.018>

SUMMARY

Most organs use fatty acids (FAs) as a key nutrient, but little is known of how blood-borne FAs traverse the endothelium to reach underlying tissues. We conducted a small-molecule screen and identified niclosamide as a suppressor of endothelial FA uptake and transport. Structure/activity relationship studies demonstrated that niclosamide acts through mitochondrial uncoupling. Inhibitors of oxidative phosphorylation and the ATP/ADP translocase also suppressed FA uptake, pointing principally to ATP production. Decreasing total cellular ATP by blocking glycolysis did not decrease uptake, indicating that specifically mitochondrial ATP is required. Endothelial FA uptake is promoted by fatty acid transport protein 4 (FATP4) via its ATP-dependent acyl-CoA synthetase activity. Confocal microscopy revealed that FATP4 resides in the endoplasmic reticulum (ER), and that endothelial ER is intimately juxtaposed with mitochondria. Together, these data indicate that mitochondrial ATP production, but not total ATP levels, drives endothelial FA uptake and transport via acyl-CoA formation in mitochondrial/ER microdomains.

INTRODUCTION

Endothelial cells (ECs) make up the innermost lining of all blood vessels (Aird, 2010). The capillary endothelium presents a barrier to the transport of solutes, particularly in those organs that harbor continuous, unfenestrated endothelium (Rose and Goresky, 1977; Sukriti et al., 2014). Fuels such as sugars and fats must therefore be actively transported across this tight barrier to the surrounding tissue. Organs like the skeletal muscle and the heart contain a continuous endothelium and rely heavily on fatty acids (FAs) as a source of fuel (Van der Vusse et al., 1998). FAs travel the bloodstream largely in two forms: esterified as triglycerides in lipoprotein particles like chylomicrons and VLDL or as free FAs non-covalently conjugated to albumin (Niot and Besnard, 2003; van der Vusse, 2009). If esterified, FAs are liberated from triglycerides by lipoprotein lipase, located on the luminal side of the endothelium (Frayn and Langin, 2003; Goldberg, 1996).

Thus, regardless of the mode of transport, FAs must cross the endothelium to reach the underlying parenchyma. Recent work has indicated that this process can be physiologically regulated in a paracrine fashion by factors secreted from the underlying tissue. For example, fat-consuming oxidative muscle fibers and cardiomyocytes secrete VEGFB, a member of the VEGF family, which then promotes FA uptake and transport in ECs (Hagberg et al., 2010). Likewise, muscle also secretes 3-hydroxy-isobutyrate (3-HIB), an intermediate catabolic product of valine, to promote trans-endothelial fatty acid transport (Jang et al., 2016). These and other regulatory mechanisms coordinate muscle metabolism with FA delivery (Arany et al., 2008).

Little is known, however, of how FAs cross the endothelial barrier in response to these physiological signals. Various mechanisms have been proposed, including paracellular transport; flip-flop into, and diffusion within, endothelial membranes; and active intracellular transport (Iso et al., 2013; Kampf et al.,

Context and Significance

Numerous tissues, including skeletal muscle, use FAs as fuel. However, excessive muscle fat content can lead to insulin resistance and type 2 diabetes. Control of fat influx into muscle is therefore important. To reach skeletal muscle, FAs must first be taken up and transported through the endothelial barrier comprising capillary walls, a process that is poorly understood. Here, researchers from the University of Pennsylvania find that perturbing mitochondrial ATP generation (but not glycolysis) in endothelial cells decreases FA uptake and transport. They also demonstrate that endothelial mitochondria line up closely with the ER, which contains FATP4, a protein that uses locally derived mitochondrial ATP to promote FA uptake. These findings open new doors for therapeutic prevention of lipid-induced insulin resistance.

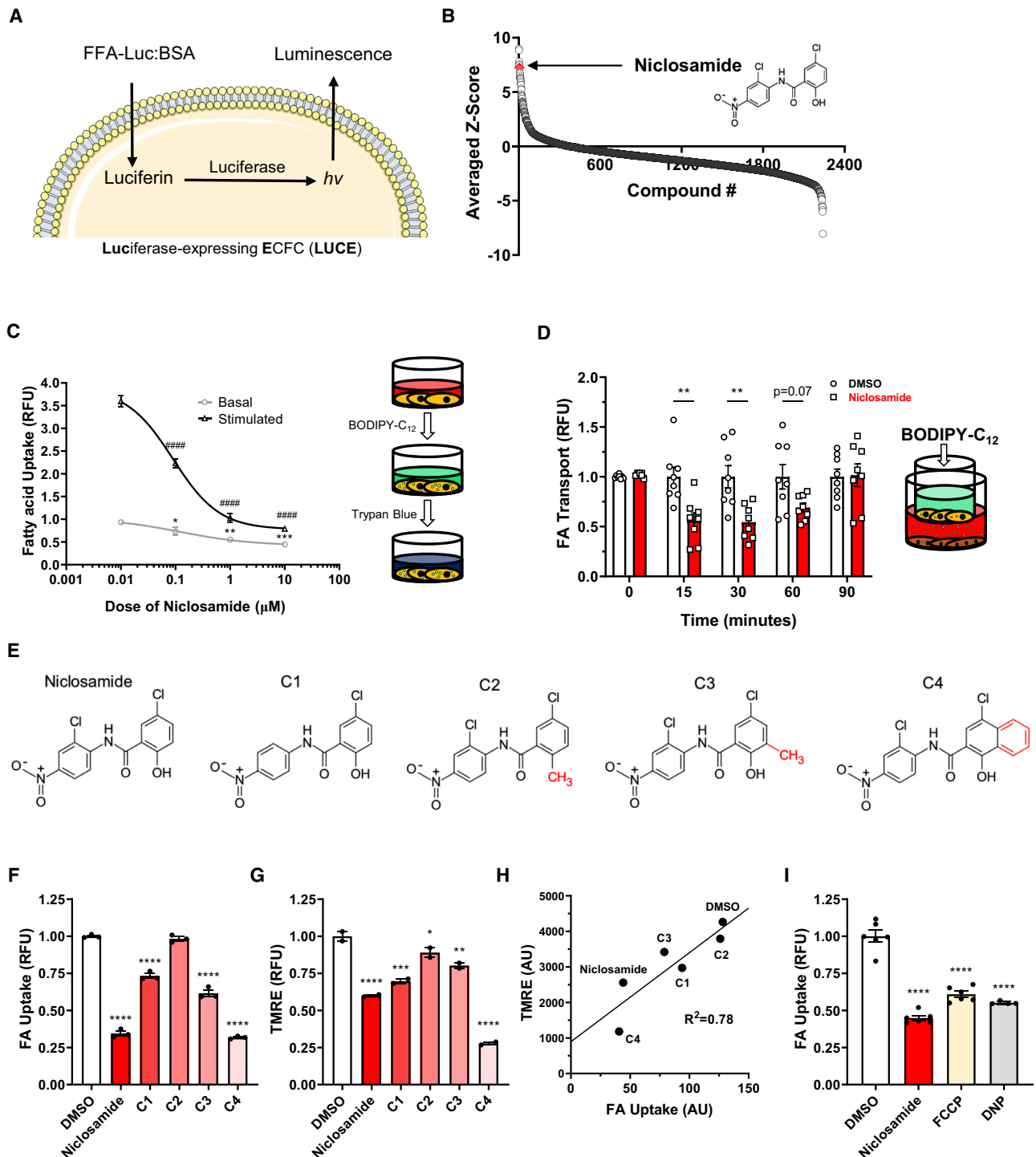


Figure 1. Chemical Screening Identifies Niclosamide as a Potent Inhibitor of Endothelial FA Uptake and Transport, Mediated via Mitochondrial Uncoupling

(A) Schematic for the luminescent FA uptake assay used for chemical screening. Palmitic acid bound via disulfide bond to luciferin is given to ECFCs expressing luciferase. The reducing environment of the cytosol frees the luciferin, which is then oxidized to produce light.

(B) Niclosamide (red diamond) ranks highly in terms of average Z score among the chemicals administered in the primary screening, indicating strong inhibition of FA uptake. The chemical structure is indicated on the right side of the graph.

(C) Dose-dependent decrease of basal and stimulated (25 mM 3-HIB) endothelial FA uptake (RFU, relative fluorescence units) in response to 1-h treatment of niclosamide. Pictured on the right is the schematic for the fluorescent BODIPY-C₁₂ based assay used to measure FA uptake.

(legend continued on next page)

2006; Komarova and Malik, 2010; Mehrotra et al., 2014; Minshall and Malik, 2006). Animals lacking endothelial CD36, a multi-functional surface receptor that facilitates FA uptake via unclear mechanisms, have significant reductions in FA uptake in heart and other organs with continuous endothelium, demonstrating that ECs present a barrier to fatty acid transport (Pepino et al., 2014; Son et al., 2018). The identification of fatty acid transport proteins (FATPs) that can promote FA import in various cell types have strengthened the argument that FA uptake is an intracellular, protein-regulated process (Anderson and Stahl, 2013; Black et al., 2009; Glatz et al., 2010; Pohl et al., 2004). In ECs, FATP3 and FATP4 are required for VEGFB-induced and 3HIB-induced FA uptake (Hagberg et al., 2010; Jang et al., 2016). However, how FATPs are regulated, and how they themselves mediate FA uptake, remains poorly understood.

Here, we undertook a high-throughput small-molecule screen to identify novel processes that mediate and control the uptake of FAs in ECs. Surprisingly, we found that endothelial mitochondria play a key role in FA uptake and transport. Specifically, the ATP produced within mitochondria, but not from glycolysis, drives the mechanism by which FATPs promote the endothelial FA uptake.

RESULTS

Niclosamide Inhibits Endothelial FA Uptake and Transport

For our small-molecule screen, we employed a luminescent FA uptake system (Henkin et al., 2012). Briefly, a compound comprised of luciferin covalently bound via a disulfide bond to palmitic acid (henceforth termed FFA-Luc) is non-covalently conjugated to bovine serum albumin (BSA) and administered to luciferase-expressing ECFCs (endothelial colony forming cells) (LUCes). Once taken up by these ECs, the FFA-Luc is cleaved by the reducing condition of the cytosol to liberate luciferin, which is then oxidized by luciferase to produce a photon. Detection of luminescence thus acts as a proxy for FA uptake (Figure 1A). Pilot experiments determined that 4 μM FFA-Luc conjugated to 3 μM BSA produced the highest Z factor ($Z' > 0.5$), using the stimulatory effects of 3-HIB as a positive control (Figure S1A). Using these concentrations, we found that the uptake of FFA-Luc occurs within seconds and plateaus at approximately 5 min (Figure S1B). Additionally, calculating the area under these curves demonstrated that LUCes increased FFA-Luc uptake over 3-fold in response to 3-HIB stimulation, indicating the robustness of the assay.

We next conducted the full chemical screen, using a library of >2,200 diverse chemical perturbagens, including kinase inhibitors, epigenetic inhibitors, GPCR/ion channel modifiers, metabolic inhibitors, microbiology agents, and FDA-approved marketed drugs with annotated biological activities, predictable activities, and proven scaffolds directed against a wide range of drug targets (Figure S1C). We delivered these compounds (and 3-HIB) in triplicate to LUCes plated onto 384-well plates and measured uptake of FFA-Luc. We identified several compounds that strongly suppressed or induced endothelial FA uptake (Figures 1B and S1D). The eight-point serial dilution curves on the top and bottom 1% (FA uptake inhibitors and activators, respectively) and testing both basal (vehicle) and stimulated (3HIB) uptake confirmed many of these hits, with several of them in the low micromolar range. One compound in particular, niclosamide, potently inhibited both basal and stimulated FA uptake during this secondary screening (Figure S1E). We next subjected these compounds to an orthogonal assay that measured uptake of the fluorescent FA analog BODIPY-C₁₂ (Figure S1F). Niclosamide again strongly suppressed FA uptake with a relative IC₅₀ of 0.1 μM for both basal and stimulated uptake (Figure 1C). Niclosamide suppressed FA uptake across a wide range of concentrations of BODIPY-C₁₂ and BSA (Figure S1G), and the suppression of FA uptake by niclosamide was rapid, achieving maximum effect within 5 min (Figure S1H). Finally, niclosamide also reduced endothelial FA transport *in vitro*, quantified by the transport of BODIPY-C₁₂ across a tight monolayer of ECs (Figure 1D).

Endothelial FA Uptake and Transport Require ATP Production

Since its discovery as an anti-helminth medication (Thompson et al., 1967), niclosamide has been observed to have effects on several molecular pathways in various cell types, including suppression of stimulatory phosphorylation of the transcription factor STAT3 (Ren et al., 2010). However, these effects are typically observed after an hour or longer, whereas we found that niclosamide decreases FA uptake within minutes (Figure S1H), suggesting a signaling-independent mechanism. More recently, Tao et al. observed that niclosamide caused rapid uncoupling of mitochondria in cell culture and *in vivo* (Tao et al., 2014). To ascertain whether mitochondrial uncoupling by niclosamide is responsible for the suppression of FA uptake in ECs, we undertook structure/activity relationship (SAR) studies, using a number of mild modifications on niclosamide's structure (Figure 1E).

(D) Kinetics of FA transport across a confluent bEnd.3 cell monolayer treated with 1 μM niclosamide. Pictured on right is the schematic for this BODIPY-C₁₂ based transport assay.

(E) Structure of niclosamide (leftmost) and chemical analogues (compounds 1 through 4, labeled C1-C4). The red-colored moiety in each of the analogues identifies their structural difference as compared to niclosamide. For C1, the difference is the absence of the chlorine that is *meta* to the nitro group in the structure of niclosamide.

(F) FA uptake in response to drugs in (E) administered for 1 h at 1 μM .

(G) Mitochondrial membrane potential as determined by flow cytometric analysis of tetramethylrhodamine ethyl ester (TMRE) signal in response to drugs in (E) administered for 1 h at 1 μM .

(H) Correlation of FA uptake and mitochondrial membrane potential in cells treated with drugs depicted in (E).

(I) FA uptake in response to three different mitochondrial uncoupling drugs for 1 h: 1 μM niclosamide, 0.5 μM FCCP, and 500 μM DNP.

BODIPY-C₁₂ and BSA were used at 2 and 1 μM , respectively, in all FA uptake assays unless otherwise specified. Data are means and error bars are \pm SEM. All statistics were determined using one-way ANOVA with Dunnett's test for multiple comparisons. * $p < 0.05$, ** $p < 0.01$, *** $p < 0.001$, **** $p < 0.0001$ (compared to DMSO-treated control); ***** $p < 0.0001$ (compared to DMSO + 3-HIB-treated control).

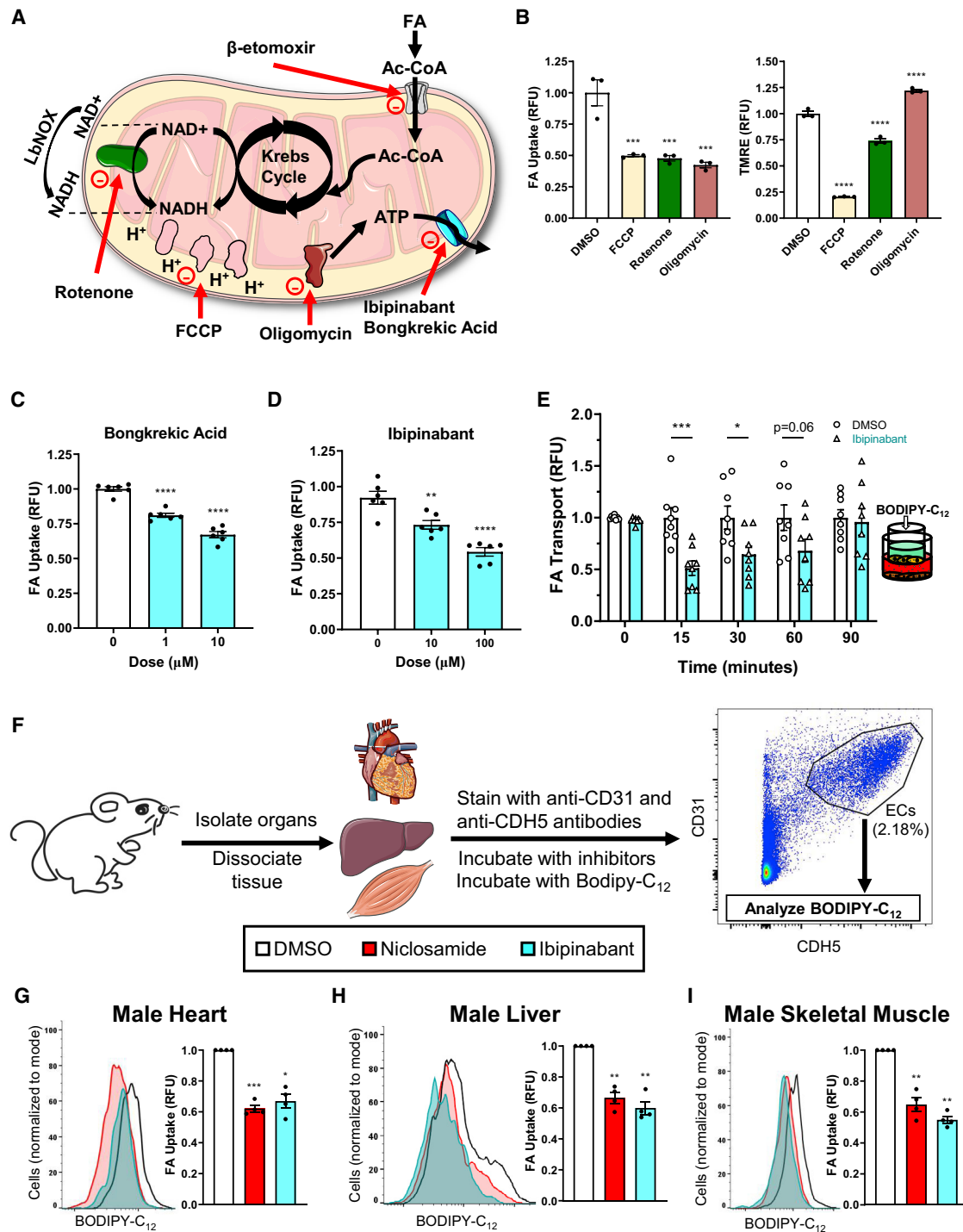


Figure 2. ATP Production Is Required for Endothelial FA Uptake *In Vitro* and *Ex Vivo*

(A) Diagram depicting the target of various mitochondrial perturbagens used below (and related Figure S2).

(B) FA uptake (left) and mitochondrial membrane potential (right) in response to 0.5 μ M FCCP, 0.5 μ M rotenone, and 1 μ M oligomycin.

(C–E) Dose-dependent FA uptake in response to ANT inhibitors bongkreikic acid (C) and ibipinabant (D). The latter drug was then tested for its effects on FA transport (E).

(F) Schematic depicting the process by which mouse ECs were identified among dissociated tissue homogenate and analyzed for FA uptake by flow cytometry. Below the schematic, a legend indicates the chemical inhibitors used and their corresponding colors in graphs (G–I) (DMSO, white; niclosamide, red; ibipinabant, cyan).

(G–I) Effects of 1-h treatment of 10 μ M niclosamide and 100 μ M ibipinabant on the FA uptake of ECs from male mouse hearts (G), livers (H), and skeletal muscle from the hindlimb (I). Median fluorescent BODIPY-C₁₂ signal was measured as a readout of FA uptake. Left of each subfigure is the corresponding representative

(legend continued on next page)

These compounds exhibited varying degrees in reduction of endothelial FA uptake, as well as varying extent of mitochondrial uncoupling, and the two functions were highly correlated (Figures 1F–1H), strongly supporting the notion that niclosamide suppresses FA uptake via uncoupling mitochondria. Furthermore, we found that two other structurally unrelated mitochondrial uncouplers, 2-[2-[4-(trifluoromethoxy)phenyl]hydrazinylidene]-propanedinitrile (FCCP) and 2,4-dinitrophenol (DNP), also strongly decreased endothelial FA uptake (Figures 1I and S1I).

To determine if other perturbations of mitochondrial function also impact FA uptake, we next tested a number of known mitochondrial inhibitors (Figure 2A). Both rotenone and oligomycin, which inhibit complex I and ATP synthase, respectively, reduced FA uptake as much as did FCCP, despite their opposing effect on the mitochondrial membrane potential (Figures 2B and S2A). Neither rotenone nor oligomycin affect endothelial migration or viability at these doses (Kim et al., 2017). These data indicated that the suppression of FA uptake does not directly rely on effects on membrane potential. Treatment with β -etomoxir, which suppresses fatty acid oxidation (FAO) by inhibiting the acyl-CoA transporter CPT1 α , had no effect on FA uptake (Figure S2B), indicating that reduced capacity for FAO does not cause suppression of FA uptake. Another possibility was the NAD⁺/NADH ratio, which is important for proper EC function (Diebold et al., 2019). However, expression of LbNOX, a bacterial enzyme that oxidizes NADH to NAD⁺ and thus increases NAD⁺/NADH, had no effect on FA uptake (Figures S2C and S2D). Together, these data suggested that no aspect of electron transport, membrane potential, or redox state was likely to fully explain the suppression of FA uptake by these reagents.

One thing that all of these perturbagens did have in common was their suppression of mitochondrial production of ATP. To test if mitochondrial ATP production was the key driver of FA uptake, we inhibited the adenine nucleotide translocator (ANT) complex, responsible for transporting mitochondrial ATP from the matrix to the cytoplasm. The structurally dissimilar ANT inhibitors bongkreic acid and ibipinabant both reduced FA uptake in a dose-dependent fashion (Figures 2C, 2D, and S2A). Moreover, ibipinabant also reduced trans-endothelial transport of FAs (Figure 2E), much like niclosamide (Figure 1D). Both niclosamide and ibipinabant had some effects on non-endothelial cell types as well, though this varied depending on the specific cell line (Figure S2E). Additionally, it is important to note that while ibipinabant also targets the CB1 receptor *CNR1* (while bongkreic acid does not), this gene is not expressed in our ECs. Taken together, these data indicate that FA uptake in ECs requires intact mitochondrial electron transport, oxidative phosphorylation, and production of ATP.

Perturbation of *Ex Vivo* Mouse Mitochondria Reduces FA Uptake

Cultured primary ECs are notoriously different from those endothelia that still reside in the mouse, having undergone significant transcriptional changes; thus, they may respond to stimuli differently than while still *in vivo*. Therefore, we carried out studies in which we harvested organs directly from mice and, within 3–4 h of sacrifice, analyzed the ECs in each sample for differences in FA uptake in response to niclosamide and ibipinabant. The organs were enzymatically dissociated, and the resultant conglomerate of cells were incubated with antibodies against the EC-specific markers CD31 and CDH5, as well as the aforementioned inhibitors. This was quickly followed by flow cytometry analysis, double gating for the endothelial markers (Figure 2F). Both niclosamide and ibipinabant reduced FA uptake in ECs from cardiac, hepatic, and skeletal muscle tissue by up to 50% (Figures 2G–2I and S2F–S2H), recapitulating *in vitro* results. Additionally, niclosamide reduced lipid droplet accumulation in ECs of *en face* aortas treated with oleic acid (Figures S2I and S2J). The requirement for mitochondrial ATP production to sustain FA uptake is thus also apparent in ECs freshly prepared *ex vivo*.

Specifically Mitochondrial ATP Production Regulates FA Uptake

The requirement of mitochondrial ATP production for endothelial FA uptake was unexpected because most of the ATP in ECs derives from glycolysis (Culic et al., 1997; De Bock et al., 2013). Indeed, 2-deoxyglucose, a competitive inhibitor of glycolysis, strongly decreased the cellular ATP/ADP ratio, whereas niclosamide and FCCP had no effect, consistent with minimal contribution of mitochondrial ATP production to overall cellular ATP (Figure 3A). However, 2-deoxyglucose had no effect on FA uptake, unlike niclosamide and FCCP (Figure 3B). AMPK activation, a frequent response to low cellular ATP/ADP ratio, also had no effect on FA uptake (Figure S3A). Glycolytic ATP production thus does not contribute to FA uptake, which appears to depend specifically on ATP emanating from mitochondria. Consistent with this conclusion, ibipinabant reduced mitochondrial ATP production by approximately 34%, as measured by the difference between the basal and oligomycin-depressed oxygen consumption rates (OCRs) (Figures 3C and 3D), with little effect on glycolysis as determined by extracellular acidification rate (ECAR) (Figure S3B), underscoring the importance of ATP derived specifically from mitochondria for FA uptake.

We next tested if, conversely, boosting ATP production specifically from mitochondria is sufficient to increase FA uptake. Monensin is a polyether ionophore that can transport monovalent cations, such as Na⁺ across lipid membranes (Lichtshtein et al., 1979). Treating cells with monensin leads to an increase in intracellular sodium, likely boosting activity from the Na⁺/K⁺

histogram. Cell number for each condition was normalized to mode. Right, bar graphs depicted such that all niclosamide or ibipinabant treated samples were measured relative to each corresponding DMSO treated sample in the same mouse (all DMSO samples were thus set to one). Four mice were used to test each organ.

BODIPY-C₁₂ and BSA were used at 2 and 1 μ M, respectively, in all FA uptake assays unless otherwise specified. For (B)–(E), data are means and error bars are \pm SEM. Statistics were determined using ordinary one-way ANOVA with Dunnett's test for multiple comparisons. For (G)–(I), data are measures of median BODIPY-C₁₂ signal and error bars are \pm SEM. Statistics were determined using paired one-way ANOVA with Dunnett's test for multiple comparisons, with DMSO controls set to one for each mouse used. * $p < 0.05$, ** $p < 0.01$, *** $p < 0.001$, **** $p < 0.0001$ (compared with DMSO treated control).

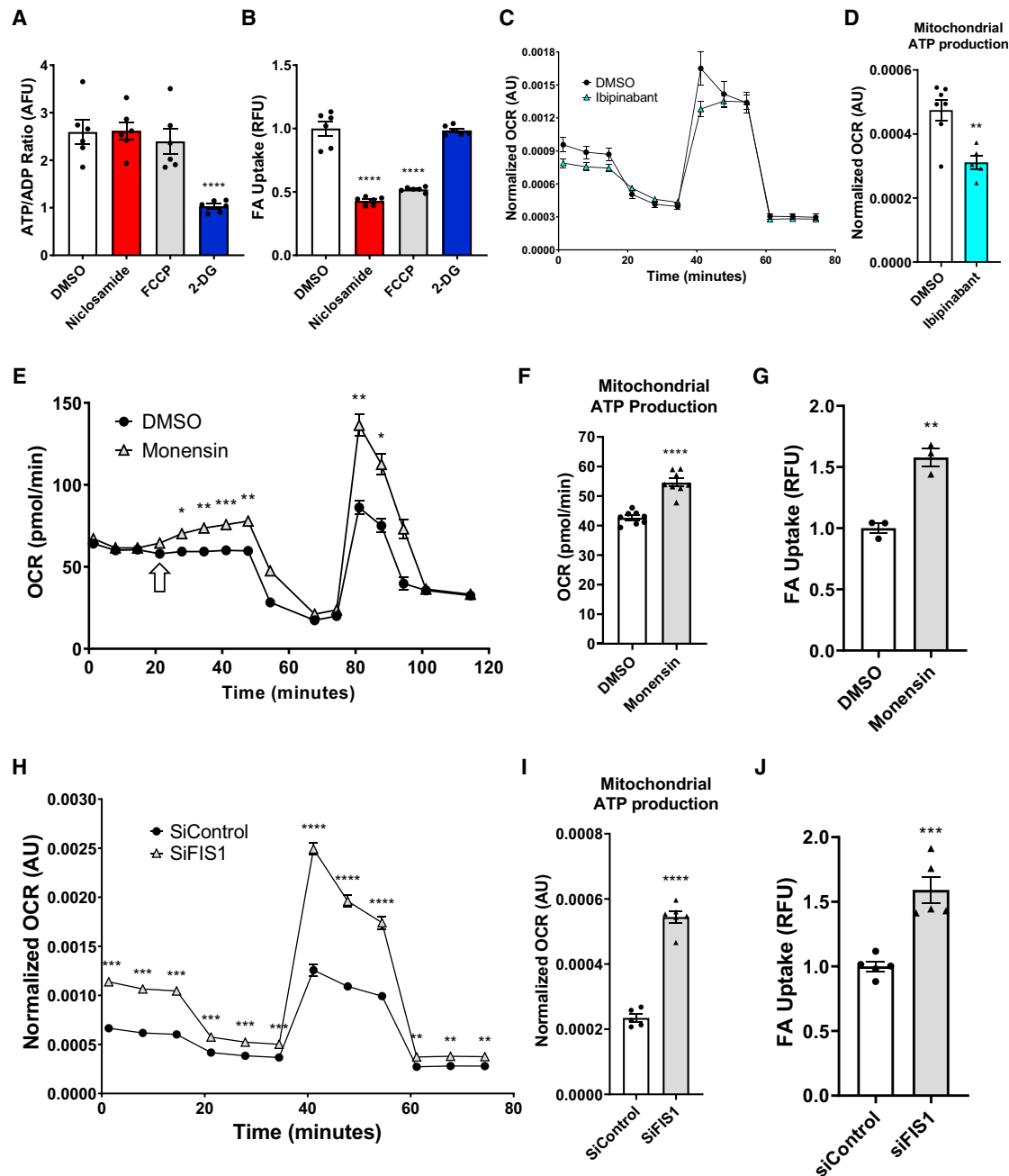


Figure 3. Specifically Mitochondrial, Not Glycolytic, ATP Production Is Necessary and Sufficient to Promote Endothelial FA Uptake

(A and B) 5.5 mM 2-deoxyglucose (2-DG) reduces cellular ATP/ADP ratio (arbitrary fluorescence units, AFU) (A) but does not affect FA uptake (B); in contrast, the uncouplers, FCCP and niclosamide, do not affect cellular ATP/ADP ratio while strongly suppressing FA uptake.

(C and D) Pre-treatment of cells with 50 μ M ibipinabant reduced basal oxygen consumption rate (OCR, normalized using CyQUANT fluorescence, arbitrary units, AU) (C) as measured during the Seahorse Mito stress test, as well as mitochondrial ATP production (D) as determined by subtraction of the oligomycin-depressed OCR from basal OCR.

(E–G) Seahorse Mito stress test modified to include a primary injection of 5 μ M monensin, which steadily increased OCR (pmol O₂ consumed per minute) (E) and mitochondrial ATP production (F). This correlates with monensin’s effect on FA uptake (G).

(H–J) 72-h KD of *FIS1* with 25 nM siRNA (siFIS1) increased overall cellular OCR (H) and mitochondrial ATP production (I) as compared with scrambled siRNA control (siControl). The same relation is seen when measuring FA uptake (J).

BODIPY-C₁₂ and BSA were used at 2 and 1 μ M, respectively, in all FA uptake assays unless otherwise specified. Data are means and error bars are \pm SEM. Statistics were determined as follows:

For (A), (B), (I), and (J), one-way ANOVA with Dunnett’s test for multiple comparisons was used. For (C), (E), and (H), two-way ANOVA with Dunnett’s test for multiple comparisons was used. For (D), (F), and (G), unpaired, two-tailed Student’s t test was used. *p < 0.05, **p < 0.01, ***p < 0.001, ****p < 0.0001 (compared with DMSO treated control or siControl).

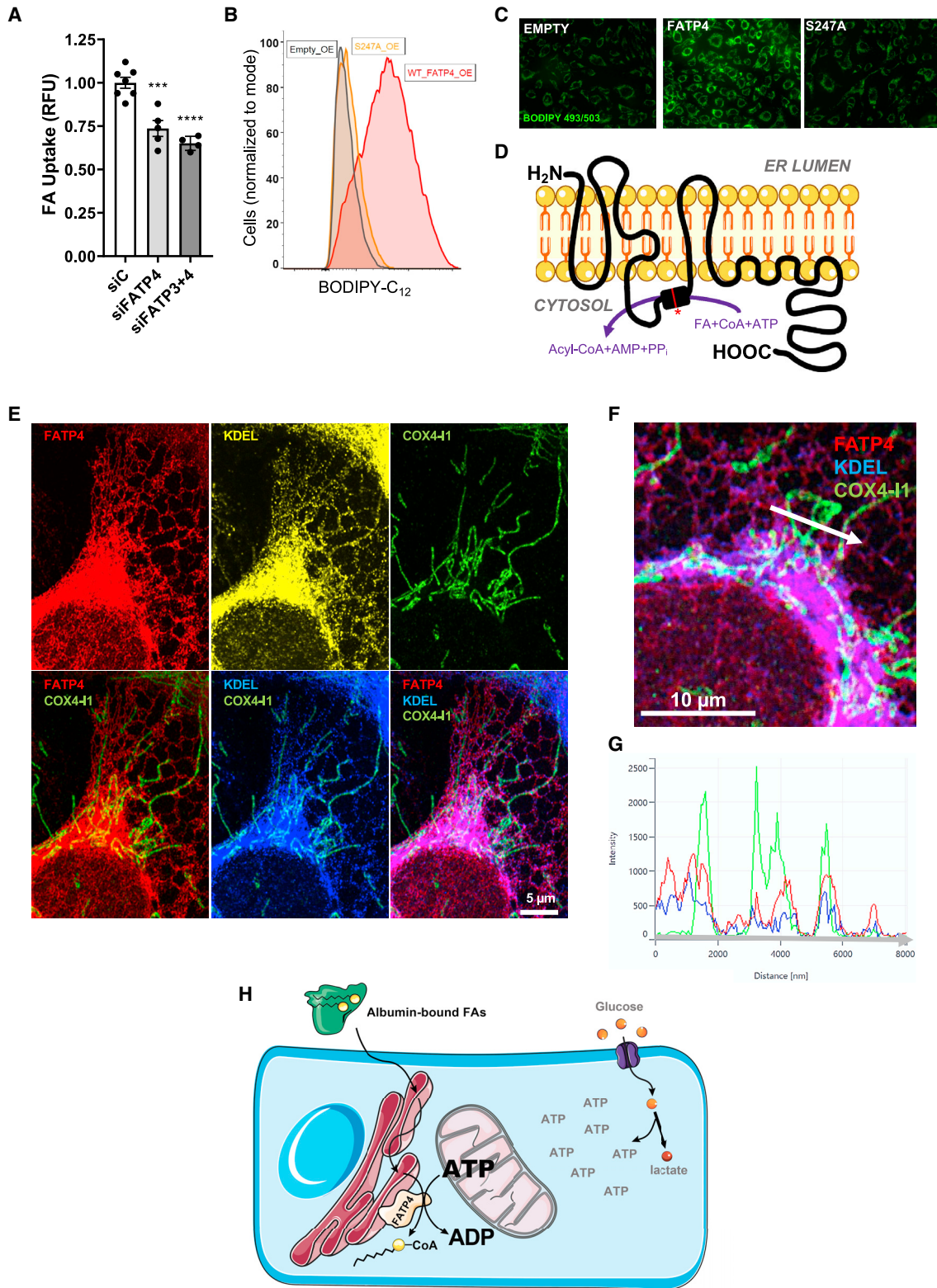


Figure 4. FATP4 Mediates Endothelial FA Uptake in a Manner Dependent on ATP and Proximity to Mitochondria
(A) 72-h KD of *FATP3* and *FATP4* with 25 nM siRNA reduced FA uptake 25%–33% as compared with scrambled control siRNA (siC).
(B) Basal FA uptake of cells overexpressing empty vector (black), wild-type *FATP4* (red), and mutant S247A *FATP4* (orange).

(legend continued on next page)

ATPase pump to export Na^+ and maintain sodium homeostasis. This higher demand for ATP then led to stimulated mitochondrial ATP production (Figures 3E and 3F). The rise in mitochondrial ATP production is accompanied by a significant increase in FA uptake (Figure 3G). Of additional importance is the fact that there was no accompanying change in ECAR (Figure S3C), nor of cellular ATP/ADP ratio (Figure S3D). Therefore, the ability of monensin to increase endothelial FA uptake likely stemmed from its effect on mitochondrial, not glycolytic, ATP production.

To further test this notion genetically, we turned to mitochondrial fusion/fission dynamics. It has been observed that cells with more fused mitochondria in general have greater production of ATP and respiratory capacity (Westermann, 2012; Yao et al., 2019). siRNA-mediated knockdown (KD) of *FIS1*, a critical fission protein, led to increased OCR in ECFCs under all conditions and increased mitochondrial ATP production as compared with those given scrambled siRNA control (Figures 3H and 3I). As with monensin, KD of *FIS1* also led to increased FA uptake (Figure 3J). KD of the fusion proteins *MFN1* and *MFN2*, which causes fragmented mitochondria, had only a minor effect on ATP production and exhibited no change in FA uptake (Figures S3E–S3G). Thus, under both pharmaceutical and genetic approaches, increasing mitochondrial ATP production leads to increased FA uptake, independently of glycolytic or overall cellular ATP.

Mitochondrial ATP Enables FATP4-Mediated Endothelial FA Uptake

The reliance on ATP specifically from mitochondria suggested both that endothelial FA uptake is an ATP-requiring process, and that it must occur in microdomains that are in close proximity to mitochondria, exclusive of glycolysis-derived ATP pools. The family of so-called FATPs have been implicated in mediating FA uptake in various cells. We and others have shown that ECs express *FATP3* and *FATP4*, and that these two transporters are required for efficient uptake of FAs (Hagberg et al., 2010; Jang et al., 2016). *FATP4*, like all FATPs, contains intrinsic ATP-dependent acyl-CoA synthetase (ACS) activity (Jia et al., 2007). siRNA-mediated KD of *FATP3* and *FATP4* led to a 33%–45% decrease in FA uptake in ECFCs (Figures 4A, S4A, and S4B). KD of ACSL1, another protein exhibiting ACS activity, also decreased FA uptake, while KD of ACSL3, ACSL4, and CD36 had no effect (Figures S4A and S4B). Conversely, overexpression of *FATP4* is sufficient to substantially increase both basal and stimulated endothelial FA uptake, as well as intracellular neutral BODIPY staining, in both human and mouse ECs, and in the presence

or absence of endogenous *FATP3/4* (Figures 4B, 4C, S4C, and S4D), and without impacting cellular respiration in the presence or absence of exogenous FAs (Figure S4E). Mutation of serine 247 to alanine in this domain renders *FATP4* unable to convert FAs to acyl-CoAs (Milger et al., 2006; Stuhlsatz-Krouper et al., 1998). Overexpression of this S247A mutant failed entirely to increase endothelial FA uptake or neutral BODIPY staining (Figures 4B, 4C, S4C, and S4D). Thus, FA uptake in ECs requires ACS activity, at least in part provided by *FATP4*, in an ATP-dependent fashion.

Based on a series of protease protection and immunofluorescence experiments, as well as hydropathy analysis, Lewis et al. proposed a topological model for murine *FATP1*, in which a single N-terminal transmembrane domain consisting of multiple helical loops is followed by an intracellular ACS domain, a peripherally associated membrane-bound section, and ending with a cytoplasmic tail (Lewis et al., 2001). Comparison of mouse *FATP1* and human *FATP4* by BLAST indicate that they are 62% identical and share 77% similarity in primary sequence (Altschul et al., 1997). Additionally, these proteins exhibit quite similar hydropathy plots (Figure S4F). Based on these facts and additional computational analyses garnered through online protein prediction software (STAR Methods), we propose a similar, hypothetical model for the topology of *FATP4* (Figure 4D). Lewis et al. proposed that the N terminus of *FATP1* lies in the extracellular space. Other studies have also indicated that *FATP1* resides in the plasma membrane under certain circumstances (Stahl et al., 2002). In contrast, using Airyscan confocal microscopy, we found that *FATP4* does not localize to the plasma membrane (Figures S4G–S4I). Instead, *FATP4* co-localizes most strongly with endothelial ER (Figure 4E), as other groups have noted in other cells (Li et al., 2013; Milger et al., 2006). Thus, *FATP4* mediates FA uptake in ECs not at the plasma membrane, but from the ER, and the N-terminal domain of *FATP4* most likely faces the lumen of the ER.

The observations that *FATP4* requires ATP to promote FA uptake, that FA uptake in ECs requires mitochondrial-derived ATP, and that *FATP4* resides in the ER all suggest that *FATP4*-containing ER networks may lie in close proximity to mitochondria. Indeed, we found striking evidence that endothelial mitochondrial networks in ECs are unerringly found in apposition to *FATP4*-containing ER (Figures 4E–4G). Using COX4-I1 as a marker of mitochondria, we find that mitochondria in ECs form extended continuous networks that are primarily perinuclear and extending into the cytoplasm but largely avoiding the periphery. COX4-I1 staining invariably coincided with KDEL staining, a marker of ER, which

(C) Overexpressing cells were incubated with 500 μM oleic acid overnight and then stained with BODIPY 493/503, which detects accumulation of neutral lipids in LDs.

(D) Proposed model for the topology of human *FATP4* in the ER membrane, based on the hydropathy analysis, software prediction, and similarity to murine *FATP1* (Lewis et al., 2001). The acyl-CoA synthetase domain (black box) mediates the conversion of FAs to acyl-CoAs at the cost of one ATP. Mutating serine 247 to alanine in this domain (the red line and asterisk) renders *FATP4* unable to promote FA uptake, as shown above.

(E) *FATP4* localizes to ER and co-localizes with mitochondria. Anti-*FATP4* antibody was used to stain *FATP4* (red, left), anti-KDEL antibody was used to stain ER (yellow and blue, middle), and anti-COX4-I1 was used to stain mitochondria (green). Scale bar, 5 μm .

(F) Overlap of mitochondrial staining (COX4-I1, green) with both *FATP4* (red) and ER (KDEL, blue) staining. Scale bar, 10 μm .

(G) Line analysis quantitation of green, red, and blue signal along the white arrow in the image depicted in (F).

(H) Model depicting the use of local mitochondrially derived ATP (separate from the glycolytic ATP pool) for *FATP4*-mediated vectorial acylation, driving endothelial FA uptake.

BODIPY- C_{12} and BSA were used at 2 and 1 μM , respectively, in all FA uptake assays unless otherwise specified. Data are means and error bars are \pm SEM. All statistics were determined using ordinary one-way ANOVA with Dunnett's test for multiple comparisons. ** $p < 0.001$, **** $p < 0.0001$ (compared with siC).

in turn is nearly identical to FATP4 staining; thus, we observed that every instance of endothelial mitochondria overlapped with the presence of FATP4 (Figures 4F and 4G). Together, these data indicate that endothelial FATP4 resides in close proximity to mitochondria and relies on locally produced mitochondrial ATP to fuel its ACS activity, thereby promoting FA uptake.

DISCUSSION

Here, we performed a small-molecule screen to glean insight into the mechanisms by which ECs take up and transport FAs. Our data led us to the conclusion that specifically mitochondrially derived ATP is required for the process of FA uptake, via provision of ATP to FATPs within microdomains of ER juxtaposed to mitochondria (Figure 4H). Importantly, ATP derived from glycolysis, the dominant source of ATP in ECs, has no impact on FA uptake.

Mitochondria have not traditionally been thought to play major roles in endothelial biology. Despite abundant access to oxygen, ECs generate >75% of their ATP via glycolysis (Culic et al., 1997; De Bock et al., 2013). Recent work, however, has demonstrated the importance of mitochondria in EC proliferation, and has suggested that the primary role of endothelial mitochondria is to serve as biosynthetic organelles for cell proliferation (Diebold et al., 2019). While proliferation of ECs is absolutely required for angiogenesis in contexts such as development or wound healing, the vast majority of ECs in adult organisms are quiescent and perform critical homeostatic tasks such as nutrient transport into underlying parenchyma. Our data demonstrate the key role that mitochondria play in such quiescent ECs.

The strong requirement for mitochondrial ATP, and of ACS activity of the FATPs and other similar proteins, is consistent with the idea of vectorial transport, a model for cellular FA uptake first hypothesized over 50 years ago (Mitchell and Moyle, 1958; Overath et al., 1969; Black and DiRusso, 2007; Arias-Barrau et al., 2009). In this model, FAs are “trapped” within the cytoplasm by enzyme-driven, ATP-dependent covalent attachment to CoA, a large hydrophilic group. The resulting “activated” acyl-CoA, now cytoplasmic, can now participate in various metabolic pathways e.g., β -oxidation or storage in lipid droplets (LDs). Moreover, this continuing shift in the equilibrium of intracellular acyl-CoA to FA promotes further FA uptake. This process is analogous to how phosphorylation of glucose to G6P not only traps the glucose in the cell but also promotes further glucose uptake (Wasserman et al., 2011; Adeva-Andany et al., 2016). The model is also consistent with the localization of FATP4 in the endothelial ER, rather than in the plasma membrane, because proximity to mitochondrial ATP is critical. In this model, access to extracellular FAs is conveyed by interconnected cellular lipid routes, i.e., the bilayer membrane network of the plasma membrane and ER. Importantly, despite their name, FATPs are unlikely to physically transport FAs, as their predicted topology does not contain channels. Indeed, in contrast to hydrophilic molecules that require active transport, the mobility of fats within the lipid bilayer is unlikely to need facilitation through aqueous channels. Instead, FATPs rely on their ACS activity to promote vectorial transport of FAs from membranes into the cytoplasm.

The fate of acyl-CoAs, once generated by FATP and other similar enzymes, is of interest and will require further study.

One possibility is that they are shuttled into the EC triglyceride pool. Sessa and colleagues have shown that a large bolus of FAs, such as with an olive oil gavage, promotes transient formation of LDs in the aortic endothelium and likely elsewhere (Kuo et al., 2017). This temporary storage of fats in the body's large EC compartment may serve to protect the underlying parenchyma from sudden surges of potentially damaging free FAs (Ibrahim and Arany, 2017). Formation of LDs requires esterification of FAs into triglycerides, a process that necessitates activation of the FAs by linkage to CoA. It will be of future interest to determine if FA transport across the endothelium obligatorily necessitates transient passage through the EC triglyceride pool.

Mitochondria have been found adjacent to the ER in multiple cell types, forming so-called mitochondrial-associated membranes (MAMs) (Raturi and Simmen, 2013; Rutter and Pinton, 2014; van Vliet and Agostinis, 2018). The exact protein components and their functions within these MAMs remains debated and are often conflicting (Brito and Scorrano, 2008; Filadi et al., 2015; Lee and Min, 2018). Our data suggest that active FATP4 may reside in such MAMs of ECs, and that a key function of these MAMs may be to create microdomains within the cytoplasm that allow for selective and local transfer of ATP without intermixing with the rest of the cytoplasm. Analogous metabolic compartmentalization can be found in metabolons: multi-enzyme complexes that channel reaction products from one enzyme to another in spatially confined multi-step metabolic processes (Srere, 1987). ECs, for example, likely contain glycolytic metabolons within lamellipodia, capable of rapid generation of ATP to sustain migration (De Bock et al., 2013; Jang and Arany, 2013). Similarly, MAMs may represent mitochondrial metabolons, capable of local generation of ATP to sustain ACS activity of FATPs and related enzymes, which in turn drive FA uptake.

In summary, we find that endothelial FA uptake and transport, a process critical to highly oxidative organs such as the skeletal muscle and heart, surprisingly depends on ATP specifically generated from mitochondria, which locally drives ATP-dependent acyl-CoA formation to promote vectorial FA transport.

Limitations of Study

Our study is limited to *in vitro* and *ex vivo* experiments in freshly isolated mouse organs, and the full physiological relevance of our findings will require further studies in intact organisms, e.g., live rodent models. Another limitation of our work is the poorly understood molecular nature of the mitochondria/ER interaction; thus, we could not successfully design experiments to interfere with that interaction. Finally, we focused on FATP4 in the ER as a paradigm for control of endothelial FA uptake, but the complete picture may be more complex. It likely includes the involvement of other acyl-CoA synthetases, possibly in subcellular locations outside of the mitochondria/ER interface.

STAR★METHODS

Detailed methods are provided in the online version of this paper and include the following:

- KEY RESOURCES TABLE

● RESOURCE AVAILABILITY

- Lead Contact
- Materials Availability
- Data and Code Availability

● EXPERIMENTAL MODEL AND SUBJECT DETAILS

- Isolation and Culture of Primary Human Endothelial Cells
- Culture of HEK293T Cells, bEnd.3 Cells, 10T1/2 and C2C12 Cells
- Culture of Adipocyte Cell Line
- Creation of LUCES
- Animal Use

● METHOD DETAILS

- RT-qPCR
- siRNA Transfection
- Retroviral Cloning
- Retroviral Over-expression
- Fatty Acid Uptake Assay of Adherent Cells
- Niclosamide Structure/Activity Relationship Studies
- Fatty Acid Transport Assay
- High Throughput Chemical Screening
- Flow Cytometric Analysis of Cultured Cells
- Flow Cytometric Analysis of *Ex Vivo* Endothelial Fatty Acid Uptake
- Oxygen Consumption and Extracellular Acidification Analysis
- CyQUANT Analysis
- ATP/ADP Ratio Analysis
- NAD⁺/NADH Ratio Analysis
- Site-Directed Mutagenesis
- Neutral Lipid Staining
- Image Acquisition and Analysis

● QUANTIFICATION AND STATISTICAL ANALYSIS

- Statistics

SUPPLEMENTAL INFORMATION

Supplemental Information can be found online at <https://doi.org/10.1016/j.cmet.2020.05.018>.

ACKNOWLEDGMENTS

We acknowledge Dr. David Schultz and Sara Cherry and the high-throughput screening core at the University of Pennsylvania for their assistance in carrying out the chemical screen. This work was supported by funding from the NIDDK (DK111091 to A.I. and DK114103 to Z.A.) and the NHLBI (HL126797 to Z.A.).

AUTHOR CONTRIBUTIONS

A.I. and Z.A. conceived the project; A.I., N.Y., and B.K. designed and carried out experiments; N.Y. assisted with the flow cytometry and the Seahorse experiments; B.K. carried out the aortic *en face* dissections, imaging studies, and the subsequent analysis; and Z.A. oversaw the project.

DECLARATION OF INTERESTS

The authors declare no competing interests.

Received: October 10, 2019

Revised: March 3, 2020

Accepted: May 18, 2020

Published: June 9, 2020

REFERENCES

- Adeva-Andany, M.M., Pérez-Felpete, N., Fernández-Fernández, C., Donapetry-García, C., and Pazos-García, C. (2016). Liver glucose metabolism in humans. *Biosci. Rep.* 36, e00416.
- Aird, W.C. (2010). Proximate and evolutionary causation of endothelial heterogeneity. *Semin. Thromb. Hemost.* 36, 276–285.
- Altschul, S.F., Madden, T.L., Schäffer, A.A., Zhang, J., Zhang, Z., Miller, W., and Lipman, D.J. (1997). Gapped BLAST and PSI-BLAST: a new generation of protein database search programs. *Nucleic Acids Res.* 25, 3389–3402.
- Anderson, C.M., and Stahl, A. (2013). SLC27 fatty acid transport proteins. *Mol. Aspects Med.* 34, 516–528.
- Arany, Z., Foo, S.Y., Ma, Y., Ruas, J.L., Bommi-Reddy, A., Girnun, G., Cooper, M., Laznik, D., Chinsomboon, J., Rangwala, S.M., et al. (2008). HIF-independent regulation of VEGF and angiogenesis by the transcriptional coactivator PGC-1 α . *Nature* 451, 1008–1012.
- Arias-Barrau, E., Dirusso, C.C., and Black, P.N. (2009). Methods to monitor fatty acid transport proceeding through vectorial acylation. *Methods Mol. Biol.* 580, 233–249.
- Black, P.N., and DiRusso, C.C. (2007). Vectorial acylation: linking fatty acid transport and activation to metabolic trafficking. *Novartis Found. Symp.* 286, 127–203.
- Black, P.N., Sandoval, A., Arias-Barrau, E., and DiRusso, C.C. (2009). Targeting the fatty acid transport proteins (FATP) to understand the mechanisms linking fatty acid transport to metabolism. *Immunol. Endocr. Metab. Agents Med. Chem.* 9, 11–17.
- Brito, O.M. de, and Scorrano, L. (2008). Mitofusin 2 tethers endoplasmic reticulum to mitochondria. *Nature* 456, 605–610.
- Buchan, D.W.A., and Jones, D.T. (2019). The PSIPRED Protein Analysis Workbench: 20 years on. *Nucleic. Acids Res.* 47, W402–W407.
- Culic, O., Gruwel, M.L., and Schrader, J. (1997). Energy turnover of vascular endothelial cells. *Am. J. Physiol.* 273, C205–C213.
- De Bock, K., Georgiadou, M., Schoors, S., Kuchnio, A., Wong, B.W., Cantelmo, A.R., Quaegebeur, A., Ghesquière, B., Cauwenberghs, S., Eelen, G., et al. (2013). Role of PFKFB3-driven glycolysis in vessel sprouting. *Cell* 154, 651–663.
- Diebold, L.P., Gil, H.J., Gao, P., Martinez, C.A., Weinberg, S.E., and Chandel, N.S. (2019). Mitochondrial complex III is necessary for endothelial cell proliferation during angiogenesis. *Nat. Metab.* 1, 158–171.
- Filadi, R., Greotti, E., Turacchio, G., Luini, A., Pozzan, T., and Pizzo, P. (2015). Mitofusin 2 ablation increases endoplasmic reticulum–mitochondria coupling. *Proc. Natl. Acad. Sci. USA* 112, E2174–E2181.
- Frayn, K.N., and Langin, D. (2003). Triacylglycerol metabolism in adipose tissue. In *Advances in Molecular and Cell Biology* (Elsevier), pp. 337–356.
- Gasteiger, E., Hoogland, C., Gattiker, A., Duvaud, S., Wilkins, M.R., Appel, R.D., and Bairoch, A. (2005). Protein identification and analysis tools on the ExPASy server. In *The Proteomics Protocols Handbook*, J.M. Walker, ed. (Humana Press), pp. 571–607.
- Glatz, J.F.C., Luiken, J.J.F.P., and Bonen, A. (2010). Membrane fatty acid transporters as regulators of lipid metabolism: implications for metabolic disease. *Physiol. Rev.* 90, 367–417.
- Goldberg, I.J. (1996). Lipoprotein lipase and lipolysis: central roles in lipoprotein metabolism and atherogenesis. *J. Lipid Res.* 37, 693–707.
- Hagberg, C.E., Falkevall, A., Wang, X., Larsson, E., Huusko, J., Nilsson, I., van Meeteren, L.A., Samen, E., Lu, L., Vanwildemeersch, M., et al. (2010). Vascular endothelial growth factor B controls endothelial fatty acid uptake. *Nature* 464, 917–921.
- Henkin, A.H., Cohen, A.S., Dubikovskaya, E.A., Park, H.M., Nikitin, G.F., Auzias, M.G., Kazantzis, M., Bertozzi, C.R., and Stahl, A. (2012). Real-time noninvasive imaging of fatty acid uptake in vivo. *ACS Chem. Biol.* 7, 1884–1891.
- Ibrahim, A., and Arany, Z. (2017). Does endothelium buffer fat? *Circ. Res.* 120, 1219–1221.

- Iso, T., Maeda, K., Hanaoka, H., Suga, T., Goto, K., Syamsunarno, M.R.A.A., Hishiki, T., Nagahata, Y., Matsui, H., Arai, M., et al. (2013). Capillary endothelial fatty acid binding Proteins 4 and 5 play a critical role in fatty acid uptake in heart and skeletal muscle. *Arterioscler. Thromb. Vasc. Biol.* **33**, 2549–2557.
- Jang, C., and Arany, Z. (2013). Metabolism: sweet enticements to move. *Nature* **500**, 409–411.
- Jang, C., Oh, S.F., Wada, S., Rowe, G.C., Liu, L., Chan, M.C., Rhee, J., Hoshino, A., Kim, B., Ibrahim, A., et al. (2016). A branched-chain amino acid metabolite drives vascular fatty acid transport and causes insulin resistance. *Nat. Med.* **22**, 421–426.
- Jia, Z., Pei, Z., Maignel, D., Toomer, C.J., and Watkins, P.A. (2007). The fatty acid transport protein (FATP) family: very long chain acyl-CoA synthetases or solute carriers? *J. Mol. Neurosci.* **33**, 25–31.
- Jones, D.T. (1999). Protein secondary structure prediction based on position-specific scoring matrices. *J. Mol. Biol.* **292**, 195–202.
- Kampf, J.P., Cupp, D., and Kleinfeld, A.M. (2006). Different mechanisms of free fatty acid flip-flop and dissociation revealed by temperature and molecular species dependence of transport across lipid vesicles. *J. Biol. Chem.* **281**, 21566–21574.
- Kim, B., Li, J., Jang, C., and Arany, Z. (2017). Glutamine fuels proliferation but not migration of endothelial cells. *EMBO J.* **36**, 2321–2333.
- Komarova, Y., and Malik, A.B. (2010). Regulation of endothelial permeability via paracellular and transcellular transport pathways. *Annu. Rev. Physiol.* **72**, 463–493.
- Kuo, A., Lee, M.Y., and Sessa, W.C. (2017). Lipid droplet biogenesis and function in the endothelium. *Circ. Res.* **120**, 1289–1297.
- Lee, S., and Min, K.T. (2018). The interface between ER and mitochondria: molecular compositions and functions. *Mol. Cells* **41**, 1000–1007.
- Lewis, S.E., Listenberger, L.L., Ory, D.S., and Schaffer, J.E. (2001). Membrane topology of the murine fatty acid transport protein 1. *J. Biol. Chem.* **276**, 37042–37050.
- Li, S., Lee, J., Zhou, Y., Gordon, W.C., Hill, J.M., Bazan, N.G., Miner, J.H., and Jin, M. (2013). Fatty acid transport protein 4 (FATP4) prevents light-induced degeneration of cone and rod photoreceptors by inhibiting RPE65 isomerase. *J. Neurosci.* **33**, 3178–3189.
- Lichtshtein, D., Dunlop, K., Kaback, H.R., and Blume, A.J. (1979). Mechanism of monensin-induced hyperpolarization of neuroblastoma-glioma hybrid NG108-15. *Proc. Natl. Acad. Sci. USA* **76**, 2580–2584.
- Lin, R.Z., and Melero-Martin, J.M. (2012). Fibroblast growth factor-2 facilitates rapid anastomosis formation between bioengineered human vascular networks and living vasculature. *Methods* **56**, 440–451.
- Mehrotra, D., Wu, J., Papangeli, I., and Chun, H.J. (2014). Endothelium as a gatekeeper of fatty acid transport. *Trends Endocrinol. Metab.* **25**, 99–106.
- Milger, K., Herrmann, T., Becker, C., Gotthardt, D., Zickwolf, J., Ehehalt, R., Watkins, P.A., Stremmel, W., and Füllekrug, J. (2006). Cellular uptake of fatty acids driven by the ER-localized acyl-CoA synthetase FATP4. *J. Cell Sci.* **119**, 4678–4688.
- Minshall, R.D., and Malik, A.B. (2006). Transport across the endothelium: regulation of endothelial permeability. *Handb. Exp. Pharmacol.* 107–144.
- Mitchell, P., and Moyle, J. (1958). Group-translocation: a consequence of enzyme-catalysed group-transfer. *Nature* **182**, 372–373.
- Niot, I., and Besnard, P. (2003). Intestinal uptake and transport of fatty acids. In *Advances in Molecular and Cell Biology* (Elsevier), pp. 9–28.
- Nugent, T., and Jones, D.T. (2009). Transmembrane protein topology prediction using support vector machines. *BMC Bioinformatics* **10**, 159.
- Overath, P., Pauli, G., and Schairer, H.U. (1969). Fatty acid degradation in *Escherichia coli*. An inducible acyl-CoA synthetase, the mapping of old-mutations, and the isolation of regulatory mutants. *Eur. J. Biochem.* **7**, 559–574.
- Pepino, M.Y., Kuda, O., Samovski, D., and Abumrad, N.A. (2014). Structure-function of CD36 and importance of fatty acid signal transduction in fat metabolism. *Annu. Rev. Nutr.* **34**, 281–303.
- Pohl, J., Ring, A., Hermann, T., and Stremmel, W. (2004). Role of FATP in parenchymal cell fatty acid uptake. *Biochim. Biophys. Acta* **1686**, 1–6.
- Raturi, A., and Simmen, T. (2013). Where the endoplasmic reticulum and the mitochondrion tie the knot: the mitochondria-associated membrane (MAM). *Biochim. Biophys. Acta* **1833**, 213–224.
- Ren, X., Duan, L., He, Q., Zhang, Z., Zhou, Y., Wu, D., Pan, J., Pei, D., and Ding, K. (2010). Identification of niclosamide as a new small-molecule inhibitor of the STAT3 signaling pathway. *ACS Med. Chem. Lett.* **1**, 454–459.
- Rose, C.P., and Goresky, C.A. (1977). Constraints on the uptake of labeled palmitate by the heart. The barriers at the capillary and sarcolemmal surfaces and the control of intracellular sequestration. *Circ. Res.* **41**, 534–545.
- Rost, B., Yachdav, G., and Liu, J. (2004). The PredictProtein server. *Nucleic Acids Res.* **32**, W321–W326.
- Rutter, G.A., and Pinton, P. (2014). Mitochondria-associated endoplasmic reticulum membranes in insulin signaling. *Diabetes* **63**, 3163–3165.
- Son, N.H., Basu, D., Samovski, D., Pietka, T.A., Peche, V.S., Willecke, F., Fang, X., Yu, S.Q., Scerbo, D., Chang, H.R., et al. (2018). Endothelial cell CD36 optimizes tissue fatty acid uptake. *J. Clin. Invest.* **128**, 4329–4342.
- Srere, P.A. (1987). Complexes of sequential metabolic enzymes. *Annu. Rev. Biochem.* **56**, 89–124.
- Stahl, A., Evans, J.G., Pattel, S., Hirsch, D., and Lodish, H.F. (2002). Insulin causes fatty acid transport protein translocation and enhanced fatty acid uptake in adipocytes. *Dev. Cell* **2**, 477–488.
- Stuhlsatz-Krouper, S.M., Bennett, N.E., and Schaffer, J.E. (1998). Substitution of alanine for serine 250 in the murine fatty acid transport protein inhibits long chain fatty acid transport. *J. Biol. Chem.* **273**, 28642–28650.
- Sukriti, S., Tauseef, M., Yazbeck, P., and Mehta, D. (2014). Mechanisms regulating endothelial permeability. *Pulm. Circ.* **4**, 535–551.
- Tao, H., Zhang, Y., Zeng, X., Shulman, G.I., and Jin, S. (2014). Niclosamide ethanolamine-induced mild mitochondrial uncoupling improves diabetic symptoms in mice. *Nat. Med.* **20**, 1263–1269.
- Thompson, C.D., Jellard, C.H., and Buckley, J.J. (1967). Human infection with a tapeworm, *Bertiella* sp., probably of African origin. *Br. Med. J.* **3**, 659–660.
- van der Vusse, G.J. (2009). Albumin as fatty acid transporter. *Drug Metab. Pharmacokinet.* **24**, 300–307.
- Van der Vusse, G.J., Glatz, J.F.C., Van Nieuwenhoven, F.A., Reneman, R.S., and Bassingthwaite, J.B. (1998). Transport of long-chain fatty acids across the muscular endothelium. In *Skeletal Muscle Metabolism in Exercise and Diabetes*, **441**, E.A. Richter, B. Kiens, H. Galbo, and B. Saltin, eds. (Springer), pp. 181–191.
- van Vliet, A.R., and Agostinis, P. (2018). Mitochondria-associated membranes and ER Stress. *Curr. Top. Microbiol. Immunol.* **414**, 73–102.
- Wada, S., Neinast, M., Jang, C., Ibrahim, Y.H., Lee, G., Babu, A., Li, J., Hoshino, A., Rowe, G.C., Rhee, J., et al. (2016). The tumor suppressor FLCN mediates an alternate mTOR pathway to regulate browning of adipose tissue. *Genes Dev.* **30**, 2551–2564.
- Wasserman, D.H., Kang, L., Ayala, J.E., Fueger, P.T., and Lee-Young, R.S. (2011). The physiological regulation of glucose flux into muscle in vivo. *J. Exp. Biol.* **214**, 254–262.
- Westermann, B. (2012). Bioenergetic role of mitochondrial fusion and fission. *Biochim. Biophys. Acta* **1817**, 1833–1838.
- Yao, C.H., Wang, R., Wang, Y., Kung, C.P., Weber, J.D., and Patti, G.J. (2019). Mitochondrial fusion supports increased oxidative phosphorylation during cell proliferation. *eLife* **8**, e41351.

STAR★METHODS

KEY RESOURCES TABLE

REAGENT or RESOURCE	SOURCE	IDENTIFIER
Antibodies		
Rabbit monoclonal anti-SLC27A4/FATP4	Abcam	Cat#Ab200353
Mouse monoclonal anti-KDEL	Abcam	Cat#Ab12223; RRID: AB_298945
Goat polyclonal anti-COX4-I1	R&D	Cat#AF5814; RRID: AB_2085286
Brilliant Violet 605 anti-mouse monoclonal CD31	BioLegend	Cat#102427; RRID: AB_2563982
CD144 (VE-cadherin) monoclonal, eFluor 660	ThermoFisher Scientific	Cat#50-1441-82; RRID: AB_11219483
Purified rat anti-mouse CD31	BD Pharmingen	Cat#553370; RRID: AB_394816
Dynabeads Sheep polyclonal anti-rat IgG	ThermoFisher Scientific	Cat#11035
Armenian Hamster anti-mouse CD31	MilliporeSigma	Cat#MAB1398Z; RRID: AB_94207
Mouse anti-human CDH5 (CD144, VE-Cadherin)	ThermoFisher Scientific	Cat#12-1449-82; RRID: AB_763438
Anti-rabbit IgG, Alexa Fluor 555	Cell Signaling Technology	Cat#4413S; RRID: AB_10694110
Anti-mouse IgG, Pacific Blue	ThermoFisher Scientific	Cat#P31582; RRID: AB_10374586
Anti-goat IgG, Alexa Fluor 488	ThermoFisher Scientific	Cat#A-11055; RRID: AB_2534102
Anti-mouse IgG, Alexa Fluor 488	ThermoFisher Scientific	Cat#4408S; RRID: AB_10694704
Anti-hamster IgG, Alexa Fluor 647	ThermoFisher Scientific	Cat#A-21451; RRID: AB_2535868
Bacterial and Virus Strains		
One Shot TOP10 Chemical Competent <i>E. coli</i>	ThermoFisher Scientific	Cat#C404003
Chemicals, Peptides, and Recombinant Proteins		
Lipofectamine RNAiMAX Transfection Reagent	ThermoFisher Scientific	Cat#13778150
Restriction enzyme: EcoRI-HF	New England BioLabs	Cat#R3101S
Restriction enzyme: XhoI	New England BioLabs	Cat#R0146S
Fugene HD Transfection Reagent	Promega	Cat#E2311
Polybrene Infection/Transfection Reagent	MilliporeSigma	Cat#TR-1003-G
Fatty acid free bovine serum albumin solution	MilliporeSigma	Cat#A9205
BODIPY FL C12	ThermoFisher Scientific	Cat#D3822
BODIPY 493/503	ThermoFisher Scientific	Cat#D3922
Dextran Texas Red, 70,000 MW, Neutral	Fisherscientific	Cat#D1830; CAS: 9004-54-0
FFA-SS-Luciferase probe	Intrace Medical	N/A
(±)-Sodium β-hydroxyisobutyrate	MilliporeSigma	Cat#36105; CAS: 1219589-99-7
Sulfo-N-succinimidyl oleate (SSO)	Cayman Chemical Company	Cat#11211; CAS: 135661-44-8 (free acid)
Tetramethylrhodamine ethyl ester perchlorate (TMRE)	MilliporeSigma	Cat#87917; CAS: 115532-52-0
4',6-diamidino-2-phenylindole (DAPI)	MilliporeSigma	Cat#D9542; CAS: 28718-90-3
Collagenase, Type I	Fisherscientific	Cat#AAJ1382003; CAS: 9001-12-1
Dispase II	MilliporeSigma	Cat#D4693; CAS: 42613-33-2
Niclosamide (Niclocide)	Selleckchem	Cat#S3030; CAS: 50-65-7
N-(2-chloro-4-nitrophenyl)-2-hydroxybenzamide (Compound 1)	Specs	AG-690/10526046; MolPort-000-639-505
5-Chloro-N-(2,6-dichloro-4-nitrophenyl)-2-methoxybenzamide (Compound 2)	Specs	AF-399/08800034; MolPort-001-667-150

(Continued on next page)

Continued

REAGENT or RESOURCE	SOURCE	IDENTIFIER
5-Chloro-N-(2,6-dichloro-4-nitrophenyl)-2-hydroxybenzamide (Compound 3)	Vitas-M Laboratory	STK055196; MolPort-000-839-501
4-chloro-N-(2-chloro-4-nitrophenyl)-1-hydroxynaphthalene-2-carboxamide (Compound 4)	Vitas-M Laboratory	STK365880; MolPort-002-319-058
Ibipinabant (SLV-319)	Cayman Chemical Company	Cat#10009226; CAS: 362519-49-1
Bongkreic Acid (ammonium salt)	Cayman Chemical Company	Cat#19079; CAS: 11076-19-0
Monensin (sodium salt)	Cayman chemical Company	Cat#16488; CAS: 22373-78-0
Carbonyl cyanide 4-(trifluoromethoxy) phenylhydrazone (FCCP)	MilliporeSigma	Cat#C2920; CAS: 370-86-5
2,4-Dinitrophenol (DNP)	MilliporeSigma	Cat#D198501; CAS: 51-28-5
Oligomycin A	MilliporeSigma	Cat#75351; CAS: 579-13-5
Rotenone	MilliporeSigma	Cat#R8875; CAS: 83-79-4
β -etomoxir	Cayman Chemical Company	Cat#11969; CAS: 828934-41-4
2-Deoxy-D-glucose	MilliporeSigma	Cat#25972; CAS: 154-17-6
5-Aminoimidazole-4-carboxamide-1- β -d-ribofuranoside (AICAR)	Cayman Chemical Company	Cat#10010241; CAS: 2627-69-2
Seahorse XF Calibrant Solution 500 mL	Agilent	Cat#100840-000
Seahorse XF base medium 500 mL	Agilent	Cat#103334-100
Seahorse XF Palmitate-BSA FAO Substrate	Agilent	Cat#102720-100
Oleic Acid-Albumin from bovine serum	MilliporeSigma	Cat#O3008; MDL: MFCD00284022
VECTASHIELD HardSet Antifade Mounting Medium	Vector Laboratories	Cat#H-1400
Selleckchem Bioactive Compound Library (96-well)	Selleckchem	L1700
Critical Commercial Assays		
Turbocapture 384 mRNA kit	Qiagen	Cat#72271
QIAEX II Gel Extraction kit	Qiagen	Cat#20021
In-Fusion HD Cloning Plus	Takara	Cat#638909
NucleoSpin Plasmid Miniprep Kit	Machery-Nagel	Cat#740588.250
Seahorse XF Cell Mito Stress Test Kit	Agilent	Cat#103015-100
ADP/ATP Ratio Bioluminescence Assay Kit, ApoSENSOR	BioVision	Cat#K255
NAD/NADH-Glo Assay	Promega	Cat#G9071
Q5 Site-Directed Mutagenesis Kit	New England BioLabs	Cat#E0552S
CyQUANT Cell Proliferation Assay	ThermoFisher Scientific	Cat#C7026
Experimental Models: Cell Lines		
Endothelial colony forming cells (ECFCs)	Obtained from pooled umbilical cord blood	N/A
Human: HEK293T cells	ATCC	CRL-3216; RRID: CVCL_0063
Mouse: bEnd.3 cells	ATCC	CRL-2299; RRID: CVCL_0170
Mouse: C2C12 cells	ATCC	CRL-1772; RRID: CVCL_0188
Mouse: 10T1/2 cells	ATCC	CCL-226; RRID: CVCL_0190
Mouse: Preadipocytes	Isolated from white adipose tissue and immortalized with SV40 TLA	Wada et al., 2016
Experimental Models: Organisms/Strains		
Mouse: C57BL/6J	The Jackson Laboratory	JAX: 000664; RRID: IMSR_JAX:000664
Oligonucleotides		
siRNA universal negative control: proprietary sequence	MilliporeSigma	Cat#SIC001
siRNA targeting human FATP3	MilliporeSigma	SASI_Hs01_00100092

(Continued on next page)

Continued

REAGENT or RESOURCE	SOURCE	IDENTIFIER
siRNA targeting human FATP4	MilliporeSigma	SASI_Hs01_00047531
siRNA targeting human FIS1	MilliporeSigma	SASI_Hs01_00171952
siRNA targeting human MFN1	MilliporeSigma	SASI_Hs01_00057999
siRNA targeting human MFN2	MilliporeSigma	SASI_Hs02_00330014
siRNA targeting mouse FATP3	MilliporeSigma	SASI_Mm01_00093273
siRNA targeting mouse FATP4	MilliporeSigma	SASI_Mm01_00151569
siRNA targeting human ACSL1	MilliporeSigma	SASI_Hs01_00202187
siRNA targeting human ACSL3	MilliporeSigma	SASI_Hs01_00034737
siRNA targeting human ACSL4	MilliporeSigma	SASI_Hs01_00114667
siRNA targeting human CD36	MilliporeSigma	SASI_Hs01_00075562
RT-qPCR primers	This paper	See Table S3
Recombinant DNA		
pMD2.G	Addgene	Cat#12259
gag/pol	Addgene	Cat#14887
psPAX2	Addgene	Cat#12260
pMSCV-Blasticidin	Addgene	Cat#75085
pUC57-LbNOX	Addgene	Cat#75285
pLenti CMV Puro LUC (w186-1)	Addgene	Cat#17477
Synthesized human FATP4 CCDS with 5' and 3' homology to pMSCV (gBlock Gene Fragments)	IDT	N/A
Software and Algorithms		
MolPort Structure Search	MolPort	https://www.molport.com/shop/index
FlowJo	FlowJo, LLC	https://www.flowjo.com/ ; RRID: SCR_008520
Graphpad Prism	Graphpad Prism	https://www.graphpad.com/scientific-software/prism/ ; RRID: SCR_002798
Zen 3.0 Blue for line profile analysis	Zeiss	https://www.zeiss.com/microscopy/us/products/microscope-software/zen.html
NCBI Protein-Protein BLAST	Altschul et al., 1997	https://blast.ncbi.nlm.nih.gov/Blast.cgi?PAGE=Proteins&
Adobe Illustrator	Adobe	https://www.adobe.com/products/illustrator.html ; RRID:SCR_010279
ExpASY ProtScale for Hydropathy Plot	Gasteiger et al., 2005	https://web.expasy.org/protscale/
PredictProtein server	Rost et al., 2004	https://www.predictprotein.org/home
PSIPRED 4.0 (Predict Secondary Structure)/MEMSAT-SVM (Membrane Helix Prediction)	Jones, 1999 ; Nugent and Jones, 2009 ; Buchan and Jones, 2019	http://bioinf.cs.ucl.ac.uk/psipred/ ; RRID: SCR_010246
Other		
Corning 96-well black polystyrene microplate	MilliporeSigma	CAT#CLS3603
Corning 6.5 mm, 0.4 μ m pore transwell inserts	MilliporeSigma	CAT#CLS3413

RESOURCE AVAILABILITY

Lead Contact

Further information and requests for resources and reagents should be directed to and will be fulfilled by the Lead Contact, Zoltan Arany (zarany@penmedicine.upenn.edu).

Materials Availability

All unique/stable reagents generated in this study are available from the Lead Contact without restriction.

Data and Code Availability

This study did not generate any unique datasets or code.

EXPERIMENTAL MODEL AND SUBJECT DETAILS

Isolation and Culture of Primary Human Endothelial Cells

Endothelial colony forming cells (ECFCs) were obtained from human umbilical cord blood as previously described (Lin and Melero-Martin, 2012). Briefly, cord blood was drawn from the umbilical vein. Mononuclear cells were separated by using Ficoll-Paque solution and plated in a dish coated with 1% gelatin. After the cells reached 80% confluency, the CD31-positive cell fraction was purified by using Dynabead-conjugated anti-CD31 capture. These were cultured on 100-mm dishes coated with 0.1% gelatin (dissolved in PBS filtered through a 0.22 μ M filter). Media used was EBM-2 with EGM-2 SingleQuots Supplements, 10% FBS and 1% Penn/Strep antibiotic solution (heretofore termed 10% EGM-2). ECFCs were used between passage 4 and 16.

Culture of HEK293T Cells, bEnd.3 Cells, 10T1/2 and C2C12 Cells

All four cell lines were obtained from ATCC and cultured with DMEM GlutaMax, 10% FBS, and 1% Penn/Strep. For the bEnd.3 cells, dishes were coated with 0.1% gelatin prior to plating. To differentiate the C2C12 cells into myotubes, they were cultured in high glucose DMEM without pyruvate, 2% horse serum, and 1% Penn/Strep.

Culture of Adipocyte Cell Line

Isolation, maintenance and differentiation of cultured adipocytes were carried out as previously described (Wada et al., 2016).

Creation of LUCes

pLenti CMV Puro LUC (w168-1) (gift from Eric Campeau & Paul Kaufman, addgene # 17477) was used as the transfer vector encoding luciferase. Virus production and spinfection onto ECFC was carried out as detailed below in Retroviral over-expression albeit with one difference: psPAX2 (gift from Didier Trono, addgene # 12260) was used as the packaging plasmid instead of gag/pol. Selection here was carried out with 10 μ g/mL puromycin. qPCR expression confirmed successful transduction. To determine functionality of the luciferase vis-à-vis fatty acid uptake, LUCes were incubated with divalent PBS or 3-HIB for one hour and then given differing concentrations of the Luc-SS-FFA reagent (complexed to differing concentrations of BSA). Resulting basal and stimulated intracellular luminescence was measured using the SpectraMax M5 microplate reader.

Animal Use

All mouse experiments were performed according to procedures approved by the University of Pennsylvania Institute for Animal Care and Use Committees (Philadelphia, PA). Mice (all of C57BL/6J genetic background) were housed under standard light/conditions. They were given food and water *ad libitum*. Both male and female mice were used; all were approximately 12-15 weeks old at time of experiment.

METHOD DETAILS

RT-qPCR

Qiagen's TurboCapture mRNA kit was used to isolate mRNA from cells and synthesize cDNA via reverse transcription. qPCR was then performed on the cDNA using the CFX384 Bio-Rad Touch Real-Time PCR Detection System and iQ SYBR Green Supermix. Primers used for mRNA analysis can be found in Table S3.

siRNA Transfection

siRNA transfections were carried out using Invitrogen's Lipofectamine RNAiMAX reagent. Cells at 70-90% confluency were kept in serum-free Opti-MEM media for the 6-hour duration of the transfection, after which they were refreshed with 10% EGM-2. Confirmation of siRNA-mediated genetic knockdown was determined using RT-qPCR.

Retroviral Cloning

LbNOX was obtained as an addgene plasmid (gift from Vamsi Mootha, addgene # 75285) while Human FATP4 cDNA was synthesized as an IDT gBlock. PCR was done to add 5' and 3' extensions that were homologous to a modified pMSCV retroviral parent vector originally obtained from addgene (gift from David Mu, addgene # 75085). The PCR products was run on a 2% agarose (in TAE buffer) gel containing 0.01% ethidium bromide. After the correct size band was excised out under UV illumination, the DNA was obtained using the Qiagen gel extraction kit.

Meanwhile, restriction digest was performed on the pMSCV parent vector using EcoR1 and Xho1 restriction enzymes (37°C, 30 minutes). This removed the filler insert and the linearized vector DNA was obtained through gel extraction as well. Ligation of

the linearized pMSCV vector and the desired insert (LbNOX or FATP4) was carried out using the Takara In-Fusion HD cloning system (50°C, 15 minutes). Transformation of the in-fusion product was carried out in Top10 chemically competent *E. coli* cells plated onto LB plates containing 50 µg/mL ampicillin. Colonies were selected, inoculated overnight, and purified via the Machery-Nagel NucleoSpin plasmid miniprep kit. The resulting purified plasmid DNA was then confirmed to be correct by submission for gene sequencing to GeneWiz.

Retroviral Over-expression

HEK293T cells were given the retroviral envelope plasmid pMD2.G (gift from Didier Trono, addgene # 12259), packaging plasmid gag/pol (gift from Tannishtha Reya, addgene # 14887) and the pMSCV transfer vector containing FATP4 or LbNOX cDNA, as well as Eugene HD Transfection Reagent. Media was refreshed the next morning. Media was collected 48- and 72-hours post-transfection; this solution contained the virus of interest and was then “spininfected” onto ECFCs. This method of transduction was carried out as follows: viral solution supplemented with 8 µg/mL polybrene was administered to 75% confluent ECFCs, after which the plate was spun in a centrifuge at 800g for 40 minutes. Immediately afterward, viral media was aspirated and 10% EGM-2 was given to cells. After one day of growth, cells were split and given fresh media containing 10 µg/mL blastomycin. Un-transduced ECFCs were also given the same media as a negative control. After 2-3 days, the latter cells were 100% dead, and survivors of the transduced cells were expanded and analyzed for expression of gene of interest via qPCR.

Fatty Acid Uptake Assay of Adherent Cells

ECFCs were plated onto Corning 96-well black-walled, clear-bottom plates (Millipore Sigma, CLS3603) at 40,000 cells/well and cultured for 48 hours or until confluent. For the assay, cells were treated with varying chemical perturbagens in divalent PBS or serum-free EGM-2 for varying times depending on the experiment, after which they were given 2 µM BODIPY-C₁₂ (with 1 µM BSA) for four minutes. After two washes with 0.1% BSA (in PBS), cells were given 0.08% Trypan Blue to quench extracellular fluorescence. Intracellular fluorescence was then swiftly measured using a Spectramax microplate reader or Synergy H1 Multi-Mode microplate reader (bottom-read, excitation: 488 nm, emission: 520 nm). Signal from wells containing cells given no BODIPY-C₁₂ was used as background noise and subtracted from experimental values.

Nicosamide Structure/Activity Relationship Studies

Compounds 1 through 4 were found and purchased through MolPort, an online software that searches for chemical compounds similar in structure to the desired parent compound (i.e., nicosamide).

Fatty Acid Transport Assay

bEnd.3 cells were seeded at 50,000 cells/transwell onto 0.4 µM inserts (pre-coated with 0.1% gelatin). Two days later, another 50,000 cells/well were seeded into the same inserts and allowed to grow for another two days. In order to ascertain that a tight monolayer of cells had formed, 70 kDa Texas-Red Dextran was added to the lower chamber of these transwells, as well as to “empty” transwells (whose inserts had been coated with gelatin but were not seeded with cells). This Dextran, being about the size of BSA, should not pass through a tight cellular monolayer as well as it passes through empty inserts. This is exactly what we observed after periodically sampling the media in the upper chamber over an hour and then reading that on a Spectramax microplate reader (bottom-read, excitation: 488 nm, emission: 520 nm).

Meanwhile, C2C12 myoblasts were differentiated into myotubes over five days. For the assay, DMSO, nicosamide or ibipinabant was added to the top chamber for one hour. Additionally, inserts were placed on top of the newly formed myotubes. The top chamber's drug solutions were then replaced with media containing 20 µM BODIPY-C₁₂ (with 10 µM BSA) while the bottom chamber was given only 10 µM BSA. The bottom chambers were sampled periodically over an hour; each sample was kept in a black-walled 96-well plate until conclusion of the assay. Finally, BODIPY-C₁₂ signal from these samples was measured using the Synergy H1 Multi-Mode microplate reader (bottom-read, excitation: 488 nm, emission: 520 nm).

High Throughput Chemical Screening

LUCs were plated onto 384-well plates at 6,000 cells per well and allowed to grow completely confluent over two days in cell culture incubators housed at the University of Pennsylvania High Throughput Screening Core. For the assay, media from each plate was aspirated and replaced by 25 µL/well divalent PBS. Immediately afterward, the SelleckChem drug library was robotically administered such that each inhibitor was present at a 1 µM concentration in each well. Columns 1 and 23 of each 384-well plate was given equivalent volume of DMSO and columns 2 and 24 were given 300 µM sulfosuccinimidyl oleate, a drug shown previously to inhibit endothelial fatty acid uptake (Jang et al., 2016). After 30 minutes, 25 µL of 50 mM 3-HIB was added to each well, resulting in a final concentration of 25 mM 3-HIB per well. After another 30 minutes, plates were loaded into the FLIPR Tetra High-Throughput Cellular Screening system. The machine then used a 384-pin pipettor head to inject 12.5 µL of a solution containing 20 µM Luc-SS-FFA and 15 µM BSA into each well of a plate simultaneously, resulting in a 4:3 µM final concentration. Reading of luminescence began within a few seconds and continued for 310 seconds. The entire chemical library was screened twice more in exactly the same manner and the resulting data was collected and analyzed by the Core. The normalized percent inhibition (NPI) and Z-score for each inhibitor was obtained and averaged across all three runs. This resulting data was plotted in Figures 1B and S1D. The raw primary screening data can be found in Table S1.

The top and bottom 20 compounds (highest and lowest average NPI, respectively), were then tested in a focused secondary screen. The methods here were very similar to those in the primary screen with two key differences. Firstly, the effects of the drugs on both basal and stimulated fatty acid uptake were tested (whereas in the primary screen, only stimulated uptake was measured as 3-HIB had been given to all samples). Secondly, dosage was tested with an 8-point serial dilution: 20, 6.67, 2.22, 0.74, 0.25, 0.08, 0.03, and 0.01 μM . The secondary screen was done in duplicate. The raw data can be found in [Table S2](#).

Flow Cytometric Analysis of Cultured Cells

ECFCs given siRNA or chemical inhibitors were incubated with 2 μM BODIPY- C_{12} (with 1 μM BSA) while still adherent. If also analyzing mitochondrial membrane potential, 75 nM TMRE was given for 15 minutes prior to incubation with BODIPY- C_{12} . 0.25% trypsin was used to lift cells off dishes and 0.1% BSA was used to wash them before centrifugation. Cells were eventually resuspended in flow buffer (comprising 0.5% BSA, 2 mM EDTA, 0.1 $\mu\text{g}/\text{mL}$ DAPI) and kept on ice until flow cytometry, which was carried out on a BD LSRII machine. Live cells were identified by gating for DAPI and choosing those events with low DAPI signal. Measure of BODIPY- C_{12} signal was used to determine fatty acid uptake. Data was analyzed on flowJo.

Flow Cytometric Analysis of Ex Vivo Endothelial Fatty Acid Uptake

12-week old male and female C57BL/6J mice were purchased from Jackson Laboratories and used over the span of three weeks for *ex vivo* work. For each run, either the heart, liver, or skeletal muscle (from the leg) from three mice were dissected and digested in 2 mg/mL collagenase and dispase in serum-free DMEM (that latter enzyme was used only for heart and skeletal muscle). Heart and liver tissue dissociated well within 20-25 minutes while skeletal muscle digestion took at least 45 minutes. All tissue homogenates were then triturated through a metal cannula and 60 mL syringe. They were then filtered through a 100- and 40-micron filter, in that order. After washing with PBS and centrifugation at 300g for five minutes, cell pellets were resuspended in 0.5% BSA in PBS and incubated with anti-CD31 (BioLegend, 102427) and anti-CD144 (ThermoFisher, 50-1441-82) antibodies for 20 minutes on ice, with gentle vortexing carried out at regular intervals. After another wash, each sample was split into three and incubated with 0.2% DMSO for 45 minutes, 10 μM niclosamide for 20 minutes, and 100 μM ibipinabant for 45 minutes at room temperature in divalent PBS. After drug incubation, all samples were washed and given 2 μM BODIPY- C_{12} (with 1 μM BSA) for four minutes. These were then washed with 0.1% BSA. After the final centrifugation, cells were resuspended in flow buffer and kept on ice until flow cytometry analysis on a BD LSRII machine. Live cells were identified by gating for DAPI. The endothelial cell population was selected by double-gating with the aforementioned antibodies, and their BODIPY- C_{12} signal was measured to determine fatty acid uptake. Data was analyzed on FlowJo.

Oxygen Consumption and Extracellular Acidification Analysis

ECFCs were plated at 40,000 cells per well onto a gelatin coated 96-well Seahorse cell culture plate and grown for 48 hours in 10% EGM-2. For the experiments using ECFCs in which *Fis1* or *MFN1+MFN2* were knocked down (or scrambled siRNA control was used), siRNA transfection was carried out on a different 100-mm dish or 6-well plate three days prior to the Seahorse assay. 1 day before the assay, these cells were split into a 96-well Seahorse cell culture plate as detailed above. As a negative control, four corners of the plate were kept devoid of cells and given only Seahorse media, which is comprised of basal XF media, 5.5 mM glucose, 1 mM sodium pyruvate, and 4 mM glutamine (additionally, the pH was adjusted to 7.4). For [Figure S4E](#), the only nutrient provided in the Seahorse media was 167 μM palmitate (conjugated to BSA, as provided by the manufacturer). At least 12 hours prior to running a plate, the Seahorse sensor cartridge was incubated with Seahorse Calibrant solution as according to manufacturer's protocol in a 37°C, CO_2 free incubator.

On the day of an assay, cells were washed and incubated with Seahorse media. For the monensin treatment and siRNA knock-down experiments ([Figures 3E, 3F, 3H, 3I, S3C, S3E, S3F, and S3H](#)), this media formulation contained no additional perturbagen. For the ANT inhibition experiment ([Figures 3C, 3D, and S3B](#)), the media contained 0.5% DMSO or 50 μM ibipinabant. The sensor cartridge was fitted onto the cell culture plate, which was then placed into a 37°C, CO_2 free incubator for one hour. During the assay, which was run on the Seahorse XF96 Analyzer, the following inhibitors were injected sequentially, as is standard for the Mito Stress Test: oligomycin (1 μM), FCCP (0.5 μM), and rotenone/antimycin (0.5 μM). For the monensin treatment experiment, 0.1% DMSO or 5 μM monensin was injected as well, prior to oligomycin injections as listed above.

CyQUANT Analysis

Data obtained from the Seahorse Oxygen Consumption and Extracellular Acidification assays done with ANT inhibition or siRNA knockdown ([Figures 3C, 3D, 3H, 3I, S3B, S3E, S3F, and S3H](#)) were normalized using ThermoFisher Scientific's fluorescent CyQUANT Kit according to manufacturer's instruction.

ATP/ADP Ratio Analysis

Cellular ATP/ADP ratio was measured using the BioVision ADP/ATP Ratio Bioluminescence Kit according to manufacturer's instruction.

NAD⁺/NADH Ratio Analysis

Cellular NAD⁺/NADH ratio was measured on ECFCs expressing LbNOX (or empty vector) using the Promega NAD/NADH-Glo Assay Kit according to manufacturer's instruction.

Site-Directed Mutagenesis

The pMSCV-based retroviral plasmid containing FATP4 was used to generate the S247A point mutant via NEB's Q5 Site-Directed Mutagenesis kit according to manufacturer's instruction.

Neutral Lipid Staining

For [Figure 4C](#), Confluent cells plated onto glass coverslips were loaded with 500 μ M oleic acid (Sigma, O3008) overnight. For [Figure S2I](#), isolated mouse aorta dissected *en face* were incubated with 500 μ M oleic acid \pm 5 μ M niclosamide overnight. The next day, samples were fixed with 3.7% paraformaldehyde, washed, permeabilized with 0.3% Triton X-100. After blocking with 2% BSA, samples were incubated with anti-mouse CD31 antibody overnight (Millipore Sigma, MAB1398Z), with secondary antibody for two hours at room temperature, and then treated with BODIPY 493/503 for 10 minutes. Finally, they were washed with PBS and mounted onto glass slides for imaging. Cells were imaged with a Nikon DS-Qi1Mc camera while aorta were imaged using the Zeiss LSM 880 with Fast Airyscan module.

Image Acquisition and Analysis

ECFCs overexpressing FATP4 were fixed in 3.7% paraformaldehyde for 10 min. After fixation, the cells were permeabilized in 0.3% Triton X-100 for 5 min and blocked with 3% BSA for 30 min. For [Figures 4E](#) and [4F](#), the cells were then incubated with primary antibodies overnight at 4°C: anti-COX4-I1 (R&D, AF5814), anti-KDEL (Abcam, ab12223), and anti-FATP4 (Abcam, ab200353). For [Figure S4H](#), cells were incubated with anti-FATP4 and anti-CDH5 (ThermoFisher Scientific, 12-1449-82). After washing with PBS, the cells were incubated with secondary antibodies for two hours at room temperature. After washing with PBS, cells were mounted with VectaShield mounting medium (VectorLabs). Imaging was done using the Zeiss LSM 880 with Fast Airyscan module (laser excitation 405 nm for KDEL, 488nm for COX4-I1 (and CDH5), and 560nm for FATP4). Image processing and the intensity values of the line profile analysis were done by using Zen 3.0 blue software.

QUANTIFICATION AND STATISTICAL ANALYSIS

Statistics

Most data in this paper are presented as mean \pm SEM. For flow cytometry experiments, BODIPY-C₁₂ signal was measured as median values. $p < 0.05$ was considered statistically significant (* $p < 0.05$, ** $p < 0.01$, *** $p < 0.001$, **** $p < 0.0001$). For comparison between two treatments, unpaired, two-tailed Student's *t* test was used. For multiple comparisons, ordinary 1-way ANOVA with Dunnett's correction was used. For the *ex vivo* experiments, paired 1-way ANOVA with Dunnett's correction was used. For the Seahorse experiments involving monensin or ibipinabant, multiple *t* tests with Dunnett's correction was used. For the Seahorse experiments involving genetic knockdown of *FIS1* and *MFN1+MFN2*, ordinary 2-way ANOVA with Dunnett's correction was used.